Journal of Marine Science and Technology (2022) 27:1015–1030
https://doi.org/10.1007/s00773-022-00890-w

ORIGINAL ARTICLE

Nonlinear observer-based adaptive output feedback tracking control of underactuated ships with input saturation

Zhipeng Shen[1] · Ang Li[1] · Li Li[1] · Haomiao Yu[1]

Received: 1 August 2021 / Accepted: 15 May 2022 / Published online: 3 June 2022

Abstract
This paper focuses on adaptive robust output feedback tracking control of an underactuated ship considering input saturation and unavailable velocities. First, a nonlinear observer is designed for the estimation of velocities and the backstepping method is combined with the dynamic surface control (DSC) technique to stabilize the tracking errors and solve the problem of complexity explosion inherent. Then, an adaptive algorithm is designed to estimate the upper bound of external disturbances. In particular, the hyperbolic tangent function and an auxiliary system are used to compensate for the input saturation. Finally, According to the Lyapunov stability theory, all closed-loop signals are uniformly ultimately bounded (UUB). Simulation results and comparisons show the effectiveness and superiority of the designed controller.

Keywords Trajectory tracking · Input saturation · Auxiliary system · Dynamic surface control · Output feedback

1 Introduction

With the rapid development of modern control theory and the advancement of intelligent control technology, some results have been achieved in complex motion control of underactuated ships [1] with multiple degrees of freedom. Unlike normal ship systems, underactuated ships are controlled only by the yaw moment of the rudder and the surge force of the propeller, so the research into underactuated ships is challenging. Moreover, because underactuated ships also have the disadvantages of strong inertia, time delay [2], and nonlinear nonlinearity [3], it is very difficult to achieve an accurate controller design. Besides, in actual navigation, the ships are vulnerable to external disturbances such as wind, waves, and currents, which will affect the motion state of the ship and cause the ship to deviate from its original course. In summary, it is meaningful to design an accurate underactuated ship controller.

In recent years, scholars have done a lot of research on the motion control of underactuated ships. Do et al. [4] used the backstepping method and Lyapunov's direct method to design the trajectory tracking control of underactuated ships. However, in the design of the backstepping method, it is necessary to derive the virtual control laws, which causes an "explosion of complexity". In [5–7], the dynamic surface control technique (DSC) was added to the backstepping, which avoided the "differential explosion" caused by the derivation of the virtual control rate and simplified the computational complexity.

In the actual sea conditions, unknown disturbances such as wind, waves and currents are inevitable, so the influence of external disturbances needs to be considered in the design of the controller. To eliminate the influence of external time-varying disturbances on ship course keeping, Liu et al. [8] designed a controller based on an adaptive sliding mode control method and a nonlinear disturbance observer, which can maintain the ship course effectively and have strong robustness against disturbances. Recently, to overcome the drawback of dependence on the model certainties, Sun et al. [9] proposed a non-deterministic adaptive control method to approximate the model uncertainties. In [10], the influence

✉ Zhipeng Shen
shenbert@dlmu.edu.cn

Ang Li
liang970202@126.com

Li Li
lili19960604@126.com

Haomiao Yu
yuhaomiao1983@163.com

1 The College of Marine Electrical Engineering, Dalian Maritime University, Dalian 116026, Liaoning, People's Republic of China

of external disturbances and the model uncertainties were eliminated by designing a fuzzy robust controller.

In general, the system status is the premise condition for controller design. However, the ship velocities are often unpredictable due to the influence of measurement noise [11], only the position and heading of the ship are measured. In [12–14], to overcome the problem of unknown velocities, output feedback control was applied to the design of the controller. In [15], a high-gain observer (HGO) was proposed to reconstruct the velocities from the measured position and heading of the ship. Ngongi et al. [16] proposed a dynamic positioning controller by integrating the HGO, the DSC technique, and the backstepping method. Considering unmeasured velocities and uncertainty parameters of the ship, a high gain observer [17, 18] provided an estimation of the ship velocities and a radial basis function (RBF) neural network compensated for the ship uncertainties. Compared with the state feedback [4], In [15–18], the design of the output feedback controllers only required position information. But the HGO has one obvious disadvantage, which is easy to generate oscillation and make the system crash. The HGO causes the peaking phenomenon [19], which leads to unexpected control performance and even system instability. Moreover, for underactuated ships, the design method of the HGO is not simple to apply directly. There is seldom research on the application of observers to underactuated ships. In [20], considering the external environment disturbances, an output feedback control law based on a linear observer is designed for the path tracking of underactuated ships. Do et al. [21] proposed a state and output feedback controller which introduces a new nonlinear observer to observe the unmeasured ship velocities. It was more robust compared with the linear controller. In [22], the unknown velocities were estimated by designing a nonlinear extended state observer which can be applied to both fully-actuated and underactuated ships.

However, the problem of ship input saturation is not considered in the above references. In the actual control process, because of the limit on system hardware and the requirement of safe driving, it is necessary to avoid the control inputs exceeding the executable range of the actuator. Therefore, input saturation [23] must be taken into account in the controller design. There are many references to input saturation in tracking control [24], position control [25], and path following control [26]. In [23], a global tracking controller was designed for underactuated ships with input and velocity constraints. To achieve dynamic positioning of the ship with disturbances and input saturation, Hu et al. [25] used a disturbance observer to estimate external disturbances and introduced the auxiliary system to solve the problem of input saturation. An adaptive control strategy of neural network (NN) based on line-of-sight (LOS) method was proposed in [26, 27]. The rudder angle with input saturation was compensated by an auxiliary system, and NN was used to approximate the model uncertainties so that the designed controller had strong robustness. The Nussbaum-type function can compensate for the time-varying nonlinear terms arising from input saturation. In [28, 29], a novel control scheme was proposed by incorporating the Nussbaum gain technique into backstepping.

Inspired by the above research, to achieve the trajectory tracking of an underactuated ship considering input saturation, unavailable velocities and unknown external disturbances, we propose an adaptive output feedback control strategy. First, a nonlinear observer is designed for the estimation of unknown ship velocities and the backstepping method is combined with the DSC technique to stabilize the tracking errors to a small neighborhood of the origin. Then, the adaptive technique is introduced to estimate the upper bound of external disturbances. The hyperbolic tangent function is introduced in the design process of control laws and the auxiliary system is also adopted to deal with the problem of input saturation. Finally, the "BAY CLASS" remote patrol ship is used as the control target. Moreover, circular and sine shapes are selected as the desired tracking trajectory to verify the effectiveness of the designed controller. The main contributions are as follows:

(1) The backstepping combined with the DSC technique solves the problem of "explosion of complexity" and avoids the singular value problem caused by the typical backstepping technique.
(2) The unmeasured velocities of the ship are estimated by introducing a nonlinear observer. A nonlinear feedback function is employed to design the observer that can effectively avoid system saturation. The Unmeasured velocities can be constructed from the position-heading measurement and the observer can suppress the noise very well.
(3) Due to the input saturation, the hyperbolic tangent function is employed to approximate the saturation function and an auxiliary system is introduced to compensate for the influence of input saturation.

The rest of this paper is organized as follows. Sect. 2 presents the problem formulation. In Sect. 3, the nonlinear observer is introduced to estimate ship velocities. Sect. 4 introduces the DSC and the backstepping techniques in controller design. In Sect. 5, the stability analysis for the designed controller. Sect. 6 completes the simulation analysis. Sect. 7 is the conclusion.

2 Problem formulation

Consider the existence of external disturbances, the kinematics and dynamics [30] of underactuated ships are described by the following differential equations:

$$\begin{aligned}\dot{\boldsymbol{\eta}} &= \boldsymbol{R}(\psi)\boldsymbol{\upsilon} \\ \boldsymbol{M}\dot{\boldsymbol{\upsilon}} &= -\boldsymbol{C}(\boldsymbol{\upsilon})\boldsymbol{\upsilon} - \boldsymbol{D}(\boldsymbol{\upsilon})\boldsymbol{\upsilon} + \boldsymbol{\tau} + \boldsymbol{\tau_w}\end{aligned} \tag{1}$$

where the vectors $\boldsymbol{\eta} = \left[x, y, \psi\right]^{\mathrm{T}}$ and $\boldsymbol{\upsilon} = [u, v, r]^{\mathrm{T}}$ denote the position (x, y), heading ψ, and the surge u, sway v, and yaw r velocities of the ship in the earth-fixed frame and the body-fixed frame. The rotation matrix in yaw $\boldsymbol{R}(\psi) = \begin{bmatrix} \cos\psi & -sin\psi & 0 \\ sin\psi & \cos\psi & 0 \\ 0 & 0 & 1 \end{bmatrix}$ describes the kinematic equation of motion, and satisfies $\boldsymbol{R}^{-1}(\psi) = \boldsymbol{R}^{\mathrm{T}}(\psi)$. The expression for Coriolis and centripetal matrix is $\boldsymbol{C}(\boldsymbol{\upsilon}) = \begin{bmatrix} 0 & 0 & -m_{22}v \\ 0 & 0 & m_{11}u \\ m_{22}v & -m_{11}u & 0 \end{bmatrix}$. The ship inertia matrix $\boldsymbol{M} = diag\left[m_{11}, m_{22}, m_{33}\right]$ includes added mass forces and moments. The hydrodynamic damping coefficients $\boldsymbol{D}(\boldsymbol{\upsilon}) = diag\left[d_{11}, d_{22}, d_{33}\right]$ consists of $d_{11}(\upsilon) = d_{u1} + d_{u2}|u|$, $d_{22}(\upsilon) = d_{v1} + d_{v2}|v|$ and $d_{33}(\upsilon) = d_{r1} + d_{r2}|r|$. The control inputs $\tau = \left[p(\tau_u), 0, p(\tau_r)\right]^{\mathrm{T}}$ consists of the surge force τ_u and yaw moment τ_r. The time-varying disturbances of the external environmental is $\tau_w = \left[\tau_{wu}, \tau_{wv}, \tau_{wr}\right]^{\mathrm{T}}$.

In the actual motion of the ship, due to the limit of propeller rotational speed and the requirement of safety, the surge force provided by the ship propeller and the yaw moment generated by the rudder are bounded which is expressed as follows:

$$p(\tau_i) = sat(\tau_i) = \begin{cases} \operatorname{sgn}(\tau_i)N_j, |\tau_i| \geq N_j \\ \tau_i, |\tau_i| < N_j \end{cases} \tag{2}$$

where $\tau_i = \left(\tau_u, \tau_r\right)$, $M_j (j = 1, 2)$ is the bound value of control input. To make the control input $p(\tau_i)$ has the nonlinear smooth characteristic, the hyperbolic tangent function is used to approximate the boundary function. The expression is as follows:

$$G(\tau_i) = N_j \tan(\frac{\tau_i}{\xi_j}) = N_j \frac{e^{\tau_i/\xi_j} - e^{-\tau_i/\xi_j}}{e^{\tau_i/\xi_j} + e^{-\tau_i/\xi_j}} \tag{3}$$

where $\xi_j (j = 1, 2)$ is the positive design parameter. The generated error function is as follows:

$$\rho(\tau_i) = sat(\tau_i) - G(\tau_i) \tag{4}$$

where $\rho(\tau_i)$ is a bounded function and its bound value is expressed as follows:

$$|\rho(\tau_i)| = |sat\left(\tau_i\right) - G(\tau_i)| \leq N_j(1 - \tanh(1)) \tag{5}$$

Assumption 1 For the desired trajectory $\left(x_d, y_d\right)$ of ship, its first derivative $\left(\dot{x}_d, \dot{y}_d\right)$ and second derivative $\left(\ddot{x}_d, \ddot{y}_d\right)$ exist and bounded.

Assumption 2 The external disturbances τ_{wu}, τ_{wv}, and τ_{wr} acting on the underactuated ships are time-varying disturbances, and satisfy $\left|\tau_{wu}\right| \leq \tau^*_{wu}$, $\left|\tau_{wv}\right| \leq \tau^*_{wv}$, and $\left|\tau_{wr}\right| \leq \tau^*_{wr}$. where $\tau^*_{wu} > 0$, $\tau^*_{wv} > 0$ and $\tau^*_{wv} > 0$ denote the upper bound of the external disturbances which are unknown constants.

Assumption 3 To facilitate the calculation and design of the controller, a simplified ship dynamics equation is used, where the inertia matrix is simplified to a diagonal matrix and the damping matrix is retained as a first-order linear and second-order non-linear damping matrix. The specific model assumptions are as follows: (a) the center of gravity coincides with the center of buoyancy ; (b) the mass distribution of the ship is homogeneous, and the ship is rigid body; (c) the heave, pitch, and roll motions are neglected; (d) The shape of the ship is symmetrical from front to back and side to side; (e) the shape structure of the vehicle is symmetrical regarding three plane of symmetrical.

3 Nonlinear observer

To eliminate the Coriolis and centripetal forces $\boldsymbol{C}(\boldsymbol{\upsilon})\boldsymbol{\upsilon}$ in Eq. 1 and facilitate the design of the nonlinear observer, a state transition matrix is introduced as follows:

$$\boldsymbol{X} = \boldsymbol{Q}(\boldsymbol{\eta})\boldsymbol{\upsilon} \tag{6}$$

where, $Q(\eta) \in R^{3\times3}$ is the generalized matrix.

Combine Eq. 1 and Eq. 6, the time derivative of X is

$$\begin{aligned}\dot{\boldsymbol{X}} = &\left(\dot{\boldsymbol{Q}}(\boldsymbol{\eta})\boldsymbol{\upsilon} - \boldsymbol{Q}(\boldsymbol{\eta})\boldsymbol{M}^{-1}\boldsymbol{C}(\boldsymbol{\upsilon})\boldsymbol{\upsilon}\right) \\ &- \boldsymbol{Q}(\boldsymbol{\eta})\boldsymbol{M}^{-1}\boldsymbol{D}(\upsilon)\boldsymbol{Q}^{-1}(\boldsymbol{\eta})X + \boldsymbol{Q}(\boldsymbol{\eta})\boldsymbol{M}^{-1}\left(\boldsymbol{\tau} + \boldsymbol{\tau}_w\right)\end{aligned} \tag{7}$$

For $\dot{\boldsymbol{Q}}(\boldsymbol{\eta})\boldsymbol{\upsilon} - \boldsymbol{Q}(\boldsymbol{\eta})\boldsymbol{M}^{-1}\boldsymbol{C}(\boldsymbol{\upsilon})\boldsymbol{\upsilon} = 0$, we have

$$\boldsymbol{Q}(\boldsymbol{\eta}) = \begin{bmatrix} cos\psi & -\frac{m_{22}}{m_{11}}\sin\psi & 0 \\ \sin\psi & \frac{m_{22}}{m_{11}}cos\psi & 0 \\ \frac{m_{11}}{m_{33}}E(\boldsymbol{\eta}) & \frac{m_{22}}{m_{33}}F(\boldsymbol{\eta}) & 1 \end{bmatrix} \tag{8}$$

where

$$\begin{aligned}E(\eta) &= x\sin\psi - y\cos\psi \\ F(\eta) &= x\cos\psi + y\sin\psi\end{aligned} \tag{9}$$

It can be obtained from the above equations that $|\boldsymbol{Q}(\boldsymbol{\eta})| = m_{22} \cdot {m_{11}}^{-1} > 0$, so $\boldsymbol{Q}(\boldsymbol{\eta})$ is a global positive definite matrix.

Substitute Eq. 8 into Eq. 7 and combine with the ship model in Eq. 1, we can get

$$\dot{\boldsymbol{\eta}} = \boldsymbol{R}(\psi)\boldsymbol{Q}^{-1}(\boldsymbol{\eta})\boldsymbol{X} \tag{10a}$$

$$\dot{\boldsymbol{X}} = -\boldsymbol{D}_\eta(\boldsymbol{\eta})\boldsymbol{X} + \boldsymbol{Q}(\boldsymbol{\eta})\boldsymbol{M}^{-1}\left(\boldsymbol{\tau} + \boldsymbol{\tau}_w\right) \tag{10b}$$

where, $\boldsymbol{D}_\eta(\boldsymbol{\eta}) = \boldsymbol{Q}(\boldsymbol{\eta})\boldsymbol{M}^{-1}\boldsymbol{D}(\boldsymbol{\upsilon})\boldsymbol{Q}^{-1}(\boldsymbol{\eta})$

Therefore, the nonlinear observer is designed as follows :

$$\dot{\hat{\boldsymbol{\eta}}} = \boldsymbol{R}(\psi)\boldsymbol{Q}^{-1}(\boldsymbol{\eta})\hat{\boldsymbol{X}} + \boldsymbol{K}_{01}\boldsymbol{G}_1(\tilde{\boldsymbol{\eta}}) \tag{11a}$$

$$\dot{\hat{\boldsymbol{X}}} = -\boldsymbol{D}_\eta(\boldsymbol{\eta})\hat{\boldsymbol{X}} + \boldsymbol{Q}(\boldsymbol{\eta})\boldsymbol{M}^{-1}\left(\boldsymbol{\tau} + \boldsymbol{\tau}_w\right) + \boldsymbol{K}_{02}\boldsymbol{G}_2(\tilde{\boldsymbol{\eta}}) \tag{11b}$$

where, $\hat{\boldsymbol{\eta}}$ and $\hat{\boldsymbol{X}}$ are the observation values of $\boldsymbol{\eta}$ and $\boldsymbol{X}$. $\boldsymbol{K}_{01}$ and $\boldsymbol{K}_{02}$ are the gain matrixes of the observer, and $\tilde{\boldsymbol{\eta}} = \boldsymbol{\eta} - \hat{\boldsymbol{\eta}}$ is the position observation error of the nonlinear observer. Nonlinear feedback functions $\boldsymbol{G}_1(\tilde{\boldsymbol{\eta}})$ and $\boldsymbol{G}_2(\tilde{\boldsymbol{\eta}})$ satisfy

$$\tilde{\boldsymbol{\eta}}^{\mathrm{T}}\boldsymbol{G}_i(\tilde{\boldsymbol{\eta}}) \geq 0, (i = 1, 2) \tag{12}$$

Select the nonlinear functions as

$$\begin{aligned}\boldsymbol{G}_1(\tilde{\boldsymbol{\eta}}) &= \left[\, g_1(\tilde{x})\ g_1(\tilde{y})\ g_1(\tilde{\psi}) \,\right]^{\mathrm{T}} \\ &= \left[\, |\tilde{x}|^{1/2}\mathrm{sign}(\tilde{x})\ |\tilde{y}|^{1/2}\mathrm{sign}(\tilde{y})\ |\tilde{\psi}|^{1/2}\mathrm{sign}(\tilde{\psi}) \,\right]^{\mathrm{T}}\end{aligned} \tag{13a}$$

$$\begin{aligned}\boldsymbol{G}_2(\tilde{\boldsymbol{\eta}}) &= \left[\, g_2(\tilde{x})\ g_2(\tilde{y})\ g_2(\tilde{\psi}) \,\right]^{T} \\ &= \left[\, |\tilde{x}|^{1/4}\mathrm{sign}(\tilde{x})\ |\tilde{y}|^{1/4}\mathrm{sign}(\tilde{y})\ |\tilde{\psi}|^{1/4}\mathrm{sign}(\tilde{\psi}) \,\right]^{\mathrm{T}}\end{aligned} \tag{13b}$$

The functions have the property of "small error but large gain, large error but small gain".

Define the observation error $\tilde{\boldsymbol{X}} = \boldsymbol{X} - \hat{\boldsymbol{X}}$ and combine Eq. 10 with Eq. 12

$$\dot{\tilde{\boldsymbol{\eta}}} = \boldsymbol{R}(\psi)\boldsymbol{Q}^{-1}(\boldsymbol{\eta})\tilde{\boldsymbol{X}} - \boldsymbol{K}_{01}\boldsymbol{G}_1(\tilde{\boldsymbol{\eta}}) \tag{14a}$$

$$\dot{\tilde{\boldsymbol{X}}} = -\boldsymbol{D}_\eta(\boldsymbol{\eta})\tilde{\boldsymbol{X}} - \boldsymbol{K}_{02}\boldsymbol{G}_2(\tilde{\boldsymbol{\eta}}) \tag{14b}$$

where, $\tilde{\boldsymbol{\eta}} = \left[\tilde{x}, \tilde{y}, \tilde{\psi}\right]^{\mathrm{T}}, \tilde{\boldsymbol{X}} = \left[\tilde{x}_1, \tilde{x}_2, \tilde{x}_3\right]^{\mathrm{T}}$.

Select Lyapunov function

$$V_0 = \frac{1}{2}\boldsymbol{G}_2(\tilde{\boldsymbol{\eta}})^{\mathrm{T}}\boldsymbol{p}_{01}\tilde{\boldsymbol{\eta}} + \frac{1}{2}\tilde{\boldsymbol{X}}^{\mathrm{T}}\boldsymbol{p}_{02}\tilde{\boldsymbol{X}} \tag{15}$$

The time derivative of V_0 is

$$\begin{aligned}\dot{V}_0 &= \boldsymbol{G}_2(\tilde{\boldsymbol{\eta}})^{\mathrm{T}}\boldsymbol{p}_{01}\dot{\tilde{\boldsymbol{\eta}}} + \tilde{\boldsymbol{X}}^{T}\boldsymbol{p}_{02}\dot{\tilde{\boldsymbol{X}}} \\ &= \boldsymbol{G}_2(\tilde{\boldsymbol{\eta}})^{\mathrm{T}}\boldsymbol{p}_{01}\Big(\boldsymbol{R}(\psi)\boldsymbol{Q}^{-1}(\boldsymbol{\eta})\tilde{\boldsymbol{X}} - \boldsymbol{K}_{01}\boldsymbol{G}_1(\tilde{\boldsymbol{\eta}})\Big) \\ &\quad + \tilde{\boldsymbol{X}}^{\mathrm{T}}\boldsymbol{p}_{02}\Big(-\boldsymbol{D}_\eta(\boldsymbol{\eta})\tilde{\boldsymbol{X}} - \boldsymbol{K}_{02}\boldsymbol{G}_2(\tilde{\boldsymbol{\eta}})\Big) \\ &= \boldsymbol{G}_2(\tilde{\boldsymbol{\eta}})^{\mathrm{T}}\boldsymbol{p}_{01}\boldsymbol{R}(\boldsymbol{\eta})\boldsymbol{Q}^{-1}(\boldsymbol{\eta})\tilde{\boldsymbol{X}} - \\ &\quad \boldsymbol{G}_2(\tilde{\boldsymbol{\eta}})^{\mathrm{T}}\boldsymbol{p}_{01}\boldsymbol{K}_{01}\boldsymbol{G}_1(\tilde{\boldsymbol{\eta}}) - \tilde{\boldsymbol{X}}^{\mathrm{T}}\boldsymbol{p}_{02}\boldsymbol{D}_\eta(\boldsymbol{\eta})\tilde{\boldsymbol{X}} \\ &\quad - \tilde{\boldsymbol{X}}^{\mathrm{T}}\boldsymbol{p}_{02}\boldsymbol{K}_{02}\boldsymbol{G}_2(\tilde{\boldsymbol{\eta}})\end{aligned} \tag{16}$$

Let $\boldsymbol{Q}_{01} = \boldsymbol{K}_{01}{}^{\mathrm{T}}\boldsymbol{p}_{01} + \boldsymbol{p}_{01}\boldsymbol{K}_{01}$ and $\boldsymbol{Q}_{02} = \boldsymbol{D}_\eta{}^{\mathrm{T}}(\boldsymbol{\eta})\boldsymbol{p}_{02} + \boldsymbol{p}_{02}\boldsymbol{D}_\eta(\boldsymbol{\eta})$, where $\boldsymbol{Q}_{01}$, $\boldsymbol{Q}_{02}$, $\boldsymbol{p}_{01}$, $\boldsymbol{p}_{02}$ and $\boldsymbol{D}_\eta(\boldsymbol{\eta})$ are positive definite matrixes, which satisfy

$$\left(\boldsymbol{R}(\psi)\boldsymbol{Q}^{-1}(\boldsymbol{\eta})\right)^{\mathrm{T}}\boldsymbol{p}_{01} - \boldsymbol{p}_{02}\boldsymbol{K}_{02} = 0 \tag{17}$$

From Eq. 12 and Eq. 13, we can get

$$\dot{V}_0 = -\frac{1}{2}\boldsymbol{G}_2(\tilde{\boldsymbol{\eta}})^{\mathrm{T}}\boldsymbol{Q}_{01}\boldsymbol{G}_1(\tilde{\boldsymbol{\eta}}) - \frac{1}{2}\tilde{\boldsymbol{X}}^{\mathrm{T}}\boldsymbol{Q}_{02}\tilde{\boldsymbol{X}} < 0 \tag{18}$$

According to Lyapunov analysis, it can be known that the nonlinear observer designed in Eq. 6 is asymptotical stable. Define the velocity estimator $\hat{\boldsymbol{\upsilon}} = \left[\hat{u}_o, \hat{v}_o, \hat{r}_o\right]^{\mathrm{T}}$ where $\hat{u}_o$, $\hat{v}_o$, and $\hat{r}_o$ are the estimation values of u, u and r respectively and satisfies

$$\hat{\boldsymbol{\upsilon}} = \boldsymbol{Q}^{-1}(\boldsymbol{\eta})\hat{\boldsymbol{X}} \tag{19}$$

The observation error $\tilde{\boldsymbol{\upsilon}} = \boldsymbol{\upsilon} - \hat{\boldsymbol{\upsilon}} = [\tilde{u}, \tilde{v}, \tilde{r}]^{\mathrm{T}}$ is defined as follows:

$$\tilde{\boldsymbol{\upsilon}} = \boldsymbol{Q}^{-1}(\boldsymbol{\eta})\tilde{\boldsymbol{X}} \tag{20}$$

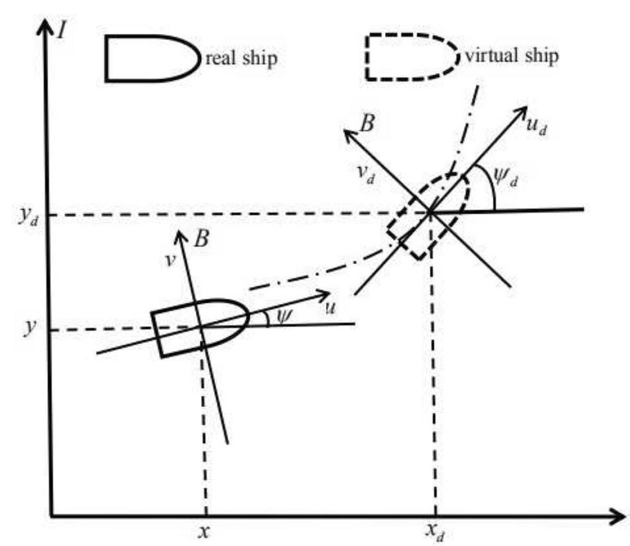

Fig. 1 Earth-fixed frame and body-fixed frame

Table 1 Model parameters of ship simulation

Parameter	Value	Parameter	Value
m_{11}	120×10^3	d_{r1}	802×10^4
m_{22}	177.9×10^9	d_{u2}	127.2×10^5
m_{33}	636×10^5	d_{v2}	43×10^2
d_{u1}	215×10^2	d_{r2}	29.4×10^3
d_{v1}	147×10^3		

Table 2 Control parameters of ship simulation

Parameter	Value	Parameter	Value	Parameter	Value
k_1	1×10^{-2}	N_1	8×10^5	σ_2	5×10^{-5}
k_2	20	N_2	1×10^7	ε_1	0.2
k_3	3	ξ_1	5	ε_1	0.05
k_4	6×10^{-5}	ξ_2	1×10^3	$\boldsymbol{p}_{01}$	$diag[1, 1, 1]$
k_5	3×10^{-2}	γ_1	1.7×10^4	$\boldsymbol{p}_{02}$	$diag[1, 1, 1]$
k_6	8×10^{-7}	γ_2	4×10^4	$\boldsymbol{K}_{01}$	$diag[1, 1, 1]$
k_7	8×10^{-7}	σ_1	5×10^{-5}		

The significance of bold values are in matrix

In summary, the observer model of the ships kinematics and dynamics shown in Eq. 1 can be expressed as

$$\dot{\hat{\boldsymbol{\eta}}} = \boldsymbol{R}(\psi)\hat{\boldsymbol{\upsilon}} + \boldsymbol{K}_{01}\boldsymbol{G}_1(\tilde{\boldsymbol{\eta}}) \tag{21a}$$

$$\boldsymbol{M}\dot{\hat{\boldsymbol{\upsilon}}} = -\boldsymbol{C}(\hat{\boldsymbol{\upsilon}})\hat{\boldsymbol{\upsilon}} - \boldsymbol{D}(\hat{\boldsymbol{\upsilon}})\hat{\boldsymbol{\upsilon}} + \boldsymbol{\tau} + \boldsymbol{\tau}_w + \boldsymbol{M}\boldsymbol{Q}^{-1}\boldsymbol{K}_{02}\boldsymbol{G}_2(\tilde{\boldsymbol{\eta}}) \tag{21b}$$

where, $\boldsymbol{K}_{01} = diag(k_{01}, k_{01}, k_{01})$ and $\boldsymbol{K}_{02} = \left(\boldsymbol{R}(\psi)\boldsymbol{Q}^{-1}\right)^{\mathrm{T}}$.

4 Controller design for trajectory tracking

4.1 Coordinate transformation and auxiliary system

$\{I\}$ is the earth-fixed frame and $\{B\}$ is the body-fixed frame in Fig. 1. The variables x_{d} and y_{d} are the desired positions of the ship. The variable ψ_{d} is the virtual ship heading angle. The variables u_{d}, v_{d}, and r_{d} are virtual ship surge, sway, and yaw velocities. The variables x_{e}, and y_{e} are the position errors in the earth-fixed frame. The variables e_x and e_y are position errors in the body-fixed frame.

To facilitate the controller design, this paper will transform the position errors x_{e} and y_{e} into e_x and e_y. Define the position and heading angle errors of the earth-fixed frame as

$$\begin{cases} x_e = x - x_d \\ y_e = y - y_d \\ \psi_e = \psi - \psi_d \end{cases} \tag{22}$$

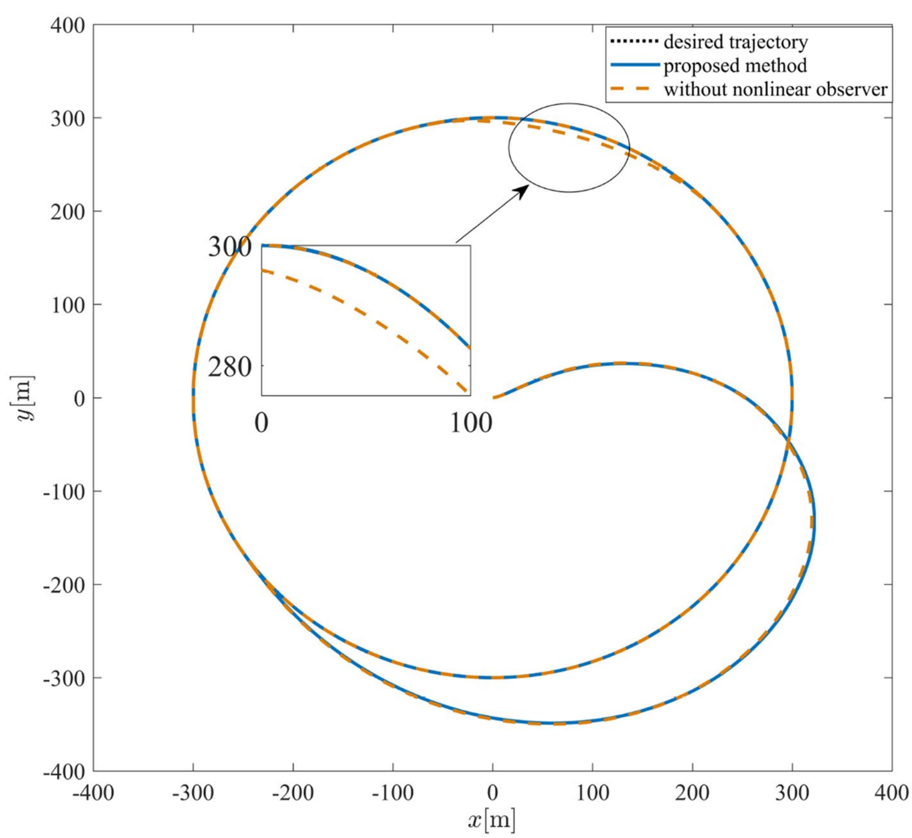

Fig. 2 Actual and desired trajectories of ship in xy-plane

Fig. 3 The curves of ship position

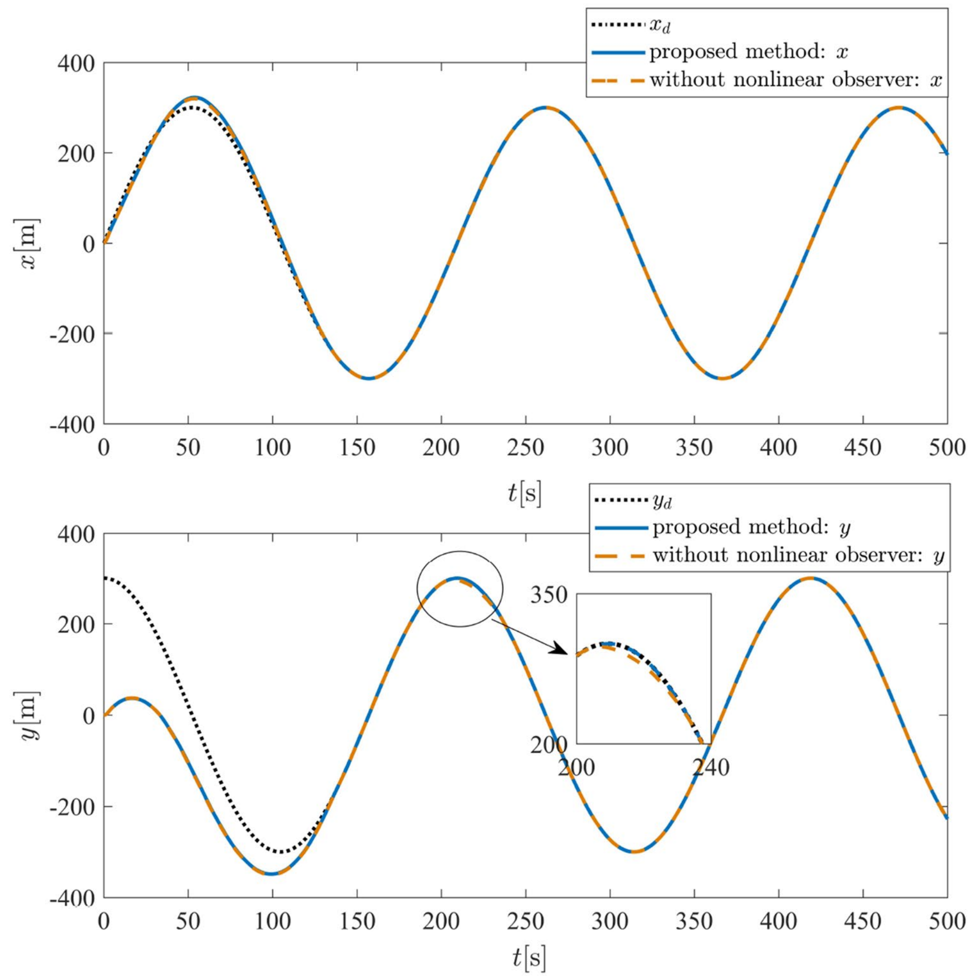

where $\psi_d = arctan\left(\frac{\dot{y}_d}{\dot{x}_d}\right)$. The ship attitude of relative desired trajectory can be determined with ψ_e.

The position errors in body-fixed frame are obtained by coordinate frame transformation

$$\begin{bmatrix} e_x \\ e_y \end{bmatrix} = \begin{bmatrix} cos\psi & sin\psi \\ -sin\psi & cos\psi \end{bmatrix} \begin{bmatrix} x_e \\ y_e \end{bmatrix} \tag{23}$$

From Eq. 23, we have $\begin{bmatrix} x_e \\ y_e \end{bmatrix} = \begin{bmatrix} cos\psi & sin\psi \\ -sin\psi & cos\psi \end{bmatrix}^{-1} \begin{bmatrix} e_x \\ e_y \end{bmatrix}$. If $\begin{cases} e_x(t) = 0 \\ e_y(t) = 0 \end{cases}$, then $\begin{cases} x_e(t) = 0 \\ y_e(t) = 0 \end{cases}$. Therefore, it is only necessary to design the control laws so that the tracking errors e_x and e_y quickly converge to a small neighborhood of the origin. From Eq. 1 and Eq. 23, the derivative of e_x and e_y are

$$\dot{e}_x = -\hat{u}_o + Ucos\psi_e + re_y \tag{24a}$$

$$\dot{e}_y = -\hat{v}_o + Usin\psi_e - re_x \tag{24b}$$

where $U = \sqrt{\dot{x}_d^2 + \dot{y}_d^2}$. Define the resultant velocity error as $\alpha = Usin\psi_e$, which can effectively avoid the singular value problems caused by the initial state constraints.

Define the velocity errors as

$$\begin{cases} u_e = \hat{u}_o - u_d \\ \alpha_e = \alpha - \alpha_d \\ r_e = \hat{r}_o - r_d \end{cases} \tag{25}$$

At the same time, to reduce the influence of the input constraints, An auxiliary system is introduced to compensate velocity errors u_e and r_e. Design the auxiliary system as

$$\dot{q}_1 = -k_6 q_1 + \frac{1}{m_{11}}\left[G(\tau_u) - \tau_u\right] \tag{26a}$$

$$\dot{q}_2 = -k_7 q_2 + \frac{1}{m_{33}}\left[G(\tau_r) - \tau_r\right] \tag{26b}$$

where k_6 and k_7 are the positive design parameters, q_1 and q_2 are the states of auxiliary system. Redefine the corrected velocity errors as

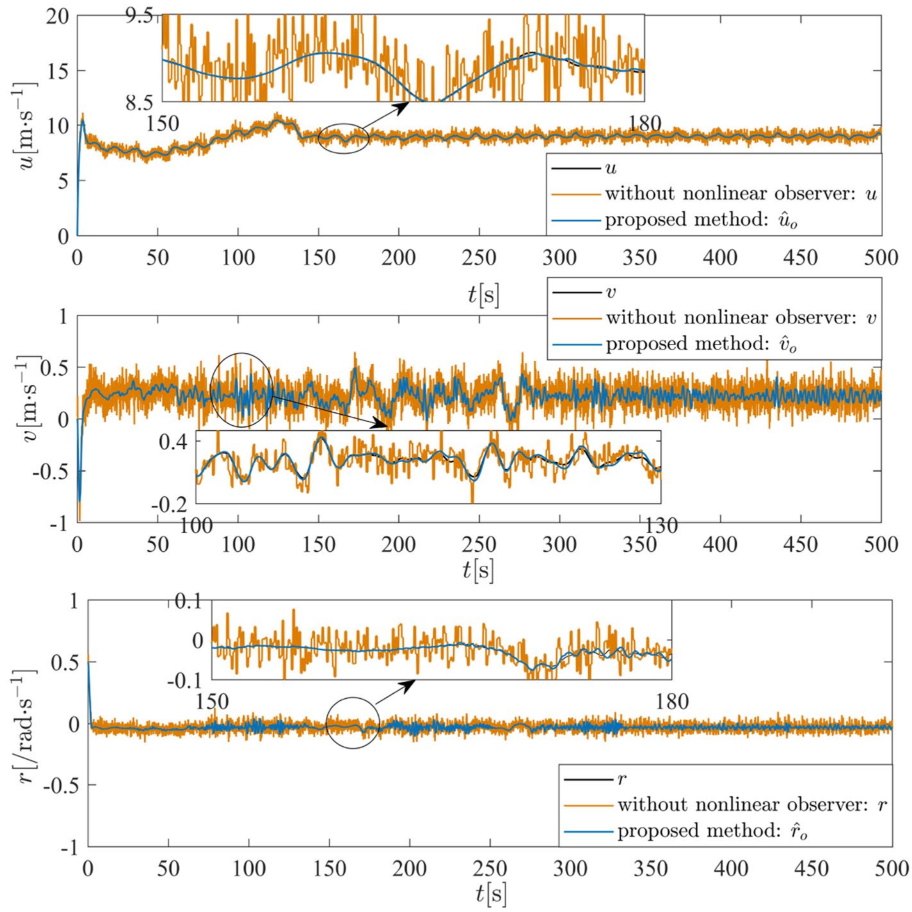

Fig. 4 The surge, sway and yaw velocities of ship

$$\bar{u}_e = u_e - q_1 \tag{27a}$$

$$\bar{r}_e = r_e - q_2 \tag{27b}$$

4.2 Controller design

The process of controller design can be divided into four steps, including stabilizing position errors e_x and e_y, stabilizing $\bar{u}_e$, stabilizing α_e and stabilizing $\bar{r}_e$.

Step 1: Stabilizing the position errors e_x and e_y. Consider the following Lyapunov function as follows:

$$V_1 = \frac{1}{2}\left(e_x^2 + e_y^2\right) \tag{28}$$

The time derivative of V_1 is

$$\begin{aligned} \dot{V}_1 &= e_x\dot{e}_x + e_y\dot{e}_y \\ &= \left(-\hat{u}_o + U\cos\psi_e\right)e_x + \left(-\hat{v}_o + \alpha\right)e_y \end{aligned} \tag{29}$$

Choose virtual control u_d and α_d as follows:

$$u_d = Ucos\psi_e + k_1e_x \tag{30a}$$

$$\alpha_d = \hat{v}_o - k_2e_y \tag{30b}$$

where k_1 and k_2 are positive design parameters.

Step 2: Stabilizing $\bar{u}_e$. Consider the following Lyapunov function

$$V_2 = V_1 + \frac{1}{2}\bar{u}_e^2 \tag{31}$$

The time derivative of V_2 is

$$\begin{aligned} \dot{V}_2 &= \dot{V}_1 + \bar{u}_e(\dot{\hat{u}}_o - \dot{u}_d - \dot{q}_1) \\ &= \dot{V}_1 + \bar{u}_e\left[\frac{1}{m_{11}}\left(m_{22}\hat{v}_o\hat{r}_o - d_{u1}\hat{u}_o - d_{u2}\hat{u}_o|\hat{u}_o| + \tau_u + \right.\right. \\ &\quad \left.\left. + \rho\left(\tau_u\right) + \tau_{wu}\right) - \dot{u}_d + k_6q_1\right] \end{aligned} \tag{32}$$

To avoid repeatedly differentiating the virtual control u_d, which will lead to the "explosion of complexity", the DSC technique is introduced [31]. Introduce a first-order filter $\boldsymbol{X_d} = [\hat{u}, \hat{\alpha}, \hat{r}]$ and let $\boldsymbol{v} = \left[u_\mathrm{d}, \alpha_d, r_d\right]$ pass through it

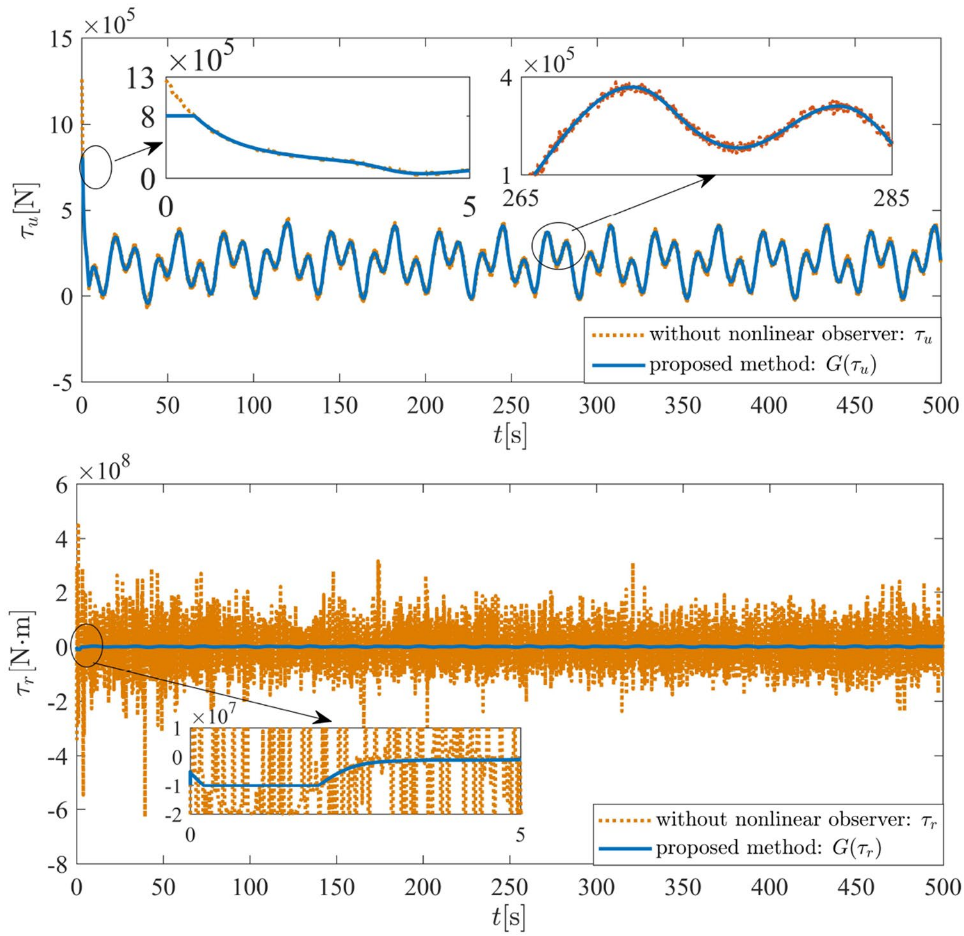

Fig. 5 The comparison curves of control inputs

$$T\dot{X}_d + X_d = v, \dot{X}_d(0) = v(0) \tag{33}$$

According to the Eq. 33, we have

$$\dot{X}_d = \left(v - X_d\right)/T \tag{34}$$

where T is the filter time constant. Define the output error of this filter as

$$Y = X_d - v \tag{35}$$

The time derivative of Y is

$$\begin{aligned}\dot{Y} = \dot{X}_d - \dot{v} = -\frac{Y}{T} + \beta_1\big(&\dot{x}_d, \ddot{x}_d, \dot{y}_d, \ddot{y}_d,\\ &e_x, \dot{e}_x, e_y, \dot{e}_y, \psi_e, \dot{\psi}_e, \dot{\psi}_d, \ddot{\psi}_d, \alpha_e, \dot{\alpha}_e\big)\end{aligned} \tag{36}$$

where β_1 is continuous function. The surge force is designed as

$$\begin{aligned}\tau_u =& m_{11}\left(\dot{\hat{u}} - k_6 q_1 - k_3\bar{u}_e - \frac{u_e e_x}{\sqrt{\bar{u}_e^2+\beta}}\right) - m_{22}\hat{v}_o\hat{r}_o\\ &+ d_{u1}\hat{u}_o + d_{u2}\hat{u}_o|\hat{u}_o| - \hat{\tau}^*_{wu}\phi\left(\bar{u}_e\right)\end{aligned} \tag{37}$$

where $\phi\left(\bar{u}_e\right) = \tanh\left(\bar{u}_e/\iota_1\right)$, k_3, k_6, ι_1 and β are positive design parameters, and $\hat{\tau}^*_{wu}$ is upper bound of the external disturbance. Design the parameter adaptive law as

$$\dot{\hat{\tau}}^*_{wu} = \gamma_1\left[\bar{u}_e\phi\left(\bar{u}_e\right) - \sigma_1\left(\hat{\tau}^*_{wu} - \tau^0_{wu}\right)\right] \tag{38}$$

where γ_1 and σ_1 are the positive design parameters, and τ^0_{wu} is a prior estimation value of $\hat{\tau}^*_{wu}$. Substitute Eq. 37 into Eq. 32

$$\begin{aligned}\dot{V}_2 =& - k_1 e_x^2 - k_2 e_y^2 - k_3\bar{u}_e^2 + \alpha_e e_y + \mu_1 + \tau^*_{wu}\\ &- \hat{\tau}^*_{wu}\phi\left(\bar{u}_e\right)\end{aligned} \tag{39}$$

where $\mu_1 = -\dfrac{\bar{u}_e u_e e_x}{\sqrt{\bar{u}_e^2 + \beta}} + u_e e_x$.

Step 3: Stabilizing α_e. Consider the following Lyapunov function

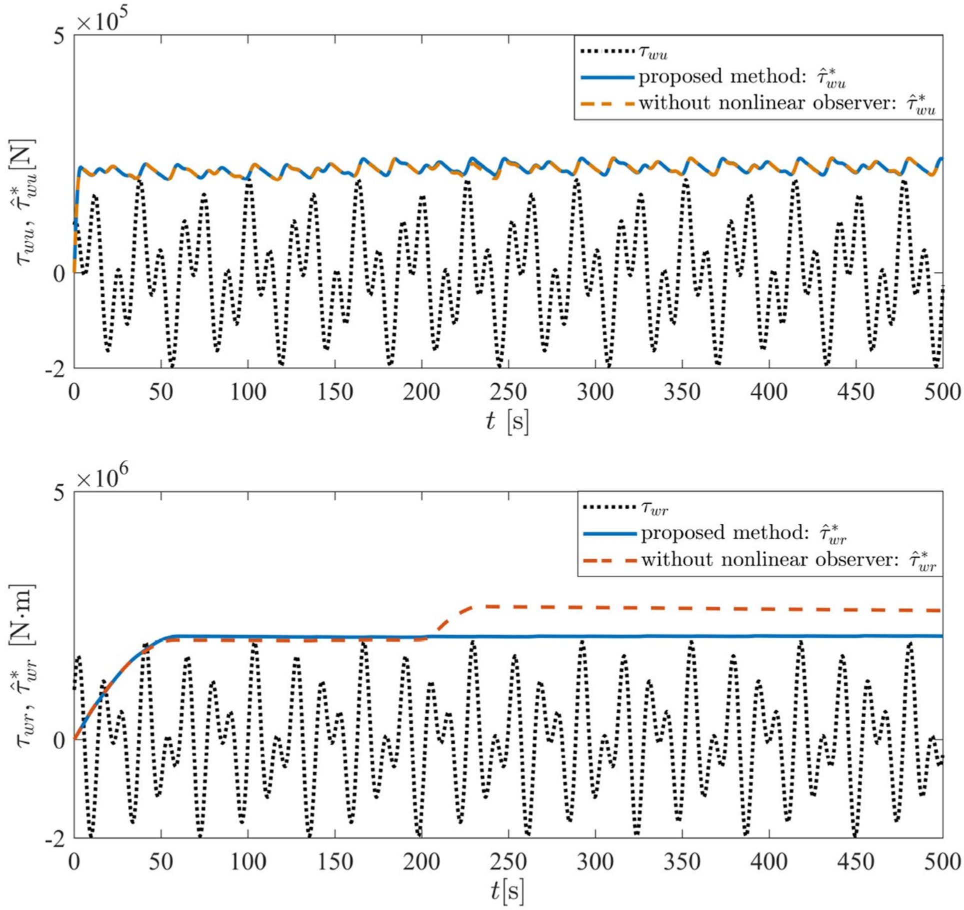

Fig. 6 External environmental disturbances and its upper bound

$$V_3 = V_2 + \frac{1}{2}\alpha_e^2 \tag{40}$$

The time derivative of V_3 is

$$\dot{V}_3 = \dot{V}_2 + \dot{\alpha}_e\alpha_e \tag{41}$$

where $\dot{\alpha}_e = \dot{U}sin\psi_e + Ucos\psi_e\left(\dot{\psi}_d - \hat{r}_o\right) - \dot{\alpha}_d$. To avoid the $\cos\left(\psi_e\right)$ appearing in the denominator when designing r_d, redefine $\widehat{r} = r\cos\left(\psi_e\right)$. Design the virtual control $\widehat{r}_{\mathrm{d}}$ as

$$\widehat{r}_d = \dot{\psi}_d\left(\cos\left(\psi_e\right) - 1\right) + r_d \tag{42}$$

Choose the virtual control r_d as follows:

$$r_d = \dot{\psi}_d + \frac{e_y + k_4\alpha_e - \dot{\alpha}_d + \dot{U}sin\psi_e}{U} \tag{43}$$

In Eq. 43, $\cos\left(\psi_e\right)$ does not appear in the denominator of r_d, which avoid the influence of $\psi_e = \frac{\pi}{2}$. The error variable is defined as follows:

$$\widehat{r}_e = \widehat{r} - \widehat{r}_d \tag{44}$$

Substitute Eq. 42 into Eq. 44, we can get

$$\begin{aligned}\widehat{r}_e &= r_e\cos\left(\psi_e\right) + \left(\cos\left(\psi_e\right) - 1\right)\left(r_d - \dot{\psi}_d\right)\\ &= r_e\cos\left(\psi_e\right) + \delta\end{aligned} \tag{45}$$

where $\delta = \left(\cos\left(\psi_e\right) - 1\right)\left(r_d - \dot{\psi}_d\right)$. Substitute Eq. 42–45 into Eq. 41

$$\begin{aligned}\dot{V}_3 = &-k_1e_x^2 - k_2e_y^2 - k_3\bar{u}_e^2 - k_4{\bar{\alpha}_e}^2 + \tau^*_{wu}\\ &-\hat{\tau}^*_{wu}\phi\left(\bar{u}_e\right) + \mu_1 + Ur_e\alpha_e\cos\left(\psi_e\right) + U\alpha_e\delta\end{aligned} \tag{46}$$

Step 4: Consider the following Lyapunov function to stabiliz $\bar{r}_e$.

$$V_4 = V_3 + \frac{1}{2}\bar{r}_e^2 \tag{47}$$

The time derivative of V_4 is

$$\begin{aligned}\dot{V}_4 &= \dot{V}_3 + \bar{r}_e\left(\dot{\hat{r}}_o - \dot{\hat{r}} - \dot{q}_2\right)\\ &= \dot{V}_3 + \bar{r}_e\left\{\frac{1}{m_{33}}\left[\tau_r + \left(m_{11} - m_{22}\right)\hat{u}_o\hat{v}_o\right.\right.\\ &\left.\left.-d_{r3}\hat{r}_o - d_{r3}\hat{r}_o|\hat{r}_o| + \rho\left(\tau_r\right)\right] - \dot{\hat{r}} + k_7q_2\right\}\end{aligned} \tag{48}$$

The yaw moment is designed as

$$\begin{aligned}\tau_r =& m_{33}(-k_5\bar{r}_e + \dot{\hat{r}} - k_7 q_2 - \frac{U\alpha_e r_e \cos\psi_e}{\sqrt{\bar{r}_e^2 + \beta}}) \\ &- (m_{11} - m_{22})\hat{u}_o\hat{v}_o + d_{r3}\hat{r}_o + d_{r3}\hat{r}_o|\hat{r}_o| - \hat{\tau}_{wr}^*\phi(\bar{r}_e)\end{aligned} \tag{49}$$

where $\phi(\bar{r}_e) = \tan(\bar{r}_e/\iota_2)$, ι_2, k_5 and k_7 are positive design parameters, and $\hat{\tau}_{wr}^*$ is upper bound of the external disturbance τ_{wr}^*.

Design parameter adaptive law as

$$\dot{\hat{\tau}}_{wr}^* = \gamma_2[\bar{r}_e\phi(\bar{r}_e) - \sigma_2(\hat{\tau}_{wr}^* - \tau_{wr}^0)] \tag{50}$$

where γ_2 and σ_2 are positive design parameters, and τ_{wr}^0 is a prior estimation of $\hat{\tau}_{\mathrm{wr}}^*$.

Substitute Eq. 49 into Eq. 48, we have

$$\begin{aligned}\dot{V}_4 =& -k_1e_x^2 - k_2e_y^2 - k_3\bar{u}_e^2 - k_4\bar{\alpha}_e{}^2 - k_5\bar{r}_e{}^2 \\ &- \hat{\tau}_{wu}^*\phi(\bar{u}_e) + \tau_{wu}^* - \hat{\tau}_{wr}^*\phi(\bar{r}_e) + \tau_{wr}^* \\ &+ U\alpha_e\delta + \mu_1 + \mu_2\end{aligned} \tag{51}$$

where $\mu_2 = -\frac{U\alpha_e r_e\bar{r}_e\cos\psi_e}{\sqrt{\bar{r}_e^2 + \beta}} + U\alpha_e r_e\cos\psi_e$.

Remark 1 The reference [5] ignored the unavailable velocities, which did not conform with the practical engineering case. This paper introduces the nonlinear observer to estimate velocities.

Remark 2 The reference [18] did not take input saturation into account in the process of controller design. When the control inputs exceed the safe range, it will cause damage to the actuator. Therefore, this paper introduces the saturation function. At the same time, an auxiliary system is introduced to reduce the influence of input saturation.

5 System stability analysis

Theorem 1 *Consider the mathematical model of underactuated ships in Eq. 1 with external disturbances and the unavailable velocities, under the control of Eq. 37 and Eq. 49 and parameter adaptive laws of Eq. 38 and Eq. 50. If the assumption 1 and 2 are satisfied, all signals in the closed-loop system are uniformly ultimately bounded (UUB) by the reasonable design of the parameters.*

Proof Consider the following Lyapunov function

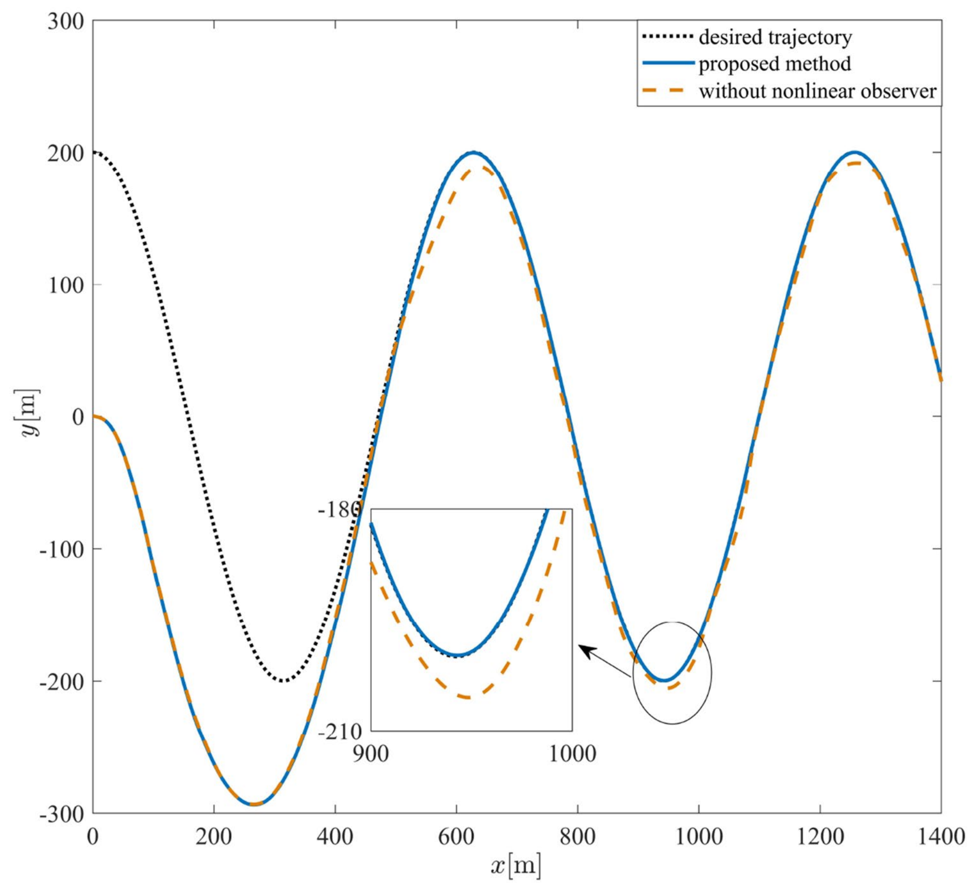

Fig. 7 Actual and desired trajectories of ship in xy-plane

$$V = V_4 + \frac{1}{2}\boldsymbol{Y}^{\mathrm{T}}\boldsymbol{Y} + \frac{1}{2\gamma_1}\tilde{\tau}_{wu}^{*2} + \frac{1}{2\gamma_2}\tilde{\tau}_{wr}^{*2} \tag{52}$$

where $\tilde{\tau}_{\mathrm{wr}}^* = \hat{\tau}_{\mathrm{wr}}^* - \tau_{\mathrm{wr}}^*$ and $\tilde{\tau}_{\mathrm{wu}}^* = \hat{\tau}_{\mathrm{wu}}^* - \tau_{\mathrm{wu}}^*$ are the disturbances estimation error.

The time derivative of V is

$$\dot{V} = \dot{V}_4 + \boldsymbol{Y}^{\mathrm{T}}\dot{\boldsymbol{Y}} + \frac{1}{\gamma_1}\dot{\hat{\tau}}_{wu}^*\tilde{\tau}_{wu}^* + \frac{1}{\gamma_2}\dot{\hat{\tau}}_{wr}^*\tilde{\tau}_{wr}^* \tag{53}$$

For given positive parameters B_0 and I_0, consider the following compact sets

$$\begin{aligned}\Omega_d = \{&(x_d, \dot{x}_d, \ddot{x}_d, y_d, \dot{y}_d, \ddot{y}_d) : \\ &x_d^2 + \dot{x}_d^2 + \ddot{x}_d^2 + y_d^2 + \dot{y}_d^2 + \ddot{y}_d^2 \le B_0\}\\ \Omega_1 = \{&(e_x, e_y, \bar{u}_e, \alpha_e, \bar{r}_e, Y, \tilde{\tau}_{wu}^*, \tilde{\tau}_{wr}^*) : V \le I_0\}\end{aligned}$$

$\Omega_d \times \Omega_1$ is also a compact set. β_1 on the compact set $\Omega_d \times \Omega_1$ has maximum N_u, so

$$\boldsymbol{Y}^{\mathrm{T}}\dot{\boldsymbol{Y}} \le -\frac{\boldsymbol{Y}^{\mathrm{T}}\boldsymbol{Y}}{T} + \omega\boldsymbol{Y}^{\mathrm{T}}\boldsymbol{Y} + \frac{N_u^2}{4\omega} \tag{54}$$

where ω is positive design parameter. Substitute Eqs. 51, 54 into Eq. 53, we have

$$\begin{aligned}\dot{V} \le &- k_1 e_x^2 - k_2 e_y^2 - k_3 \bar{u}_e^2 - k_4 \alpha_e^2 - k_5 \bar{r}_e^2\\ &+ \tau_{wu}^*[|\bar{u}_e| - \bar{u}_e\phi(\bar{u}_e)] + \tau_{wr}^*[|\bar{r}_e| - \bar{r}_e\phi(\bar{r}_e)]\\ &+ \sigma_1(\tau_{wu}^* - \hat{\tau}_{wu}^*)(\hat{\tau}_{wu}^* - \tau_{wu}^0) + U\alpha_e\delta\\ &+ \sigma_2(\tau_{wr}^* - \hat{\tau}_{wr}^*)(\hat{\tau}_{wr}^* - \tau_{wr}^0) + \mu_1 + \mu_2\\ &- \left(\frac{1}{T} - \omega\right)\boldsymbol{Y}^{\mathrm{T}}\boldsymbol{Y} + \frac{N_u^2}{4\omega} + 1\end{aligned} \tag{55}$$

Consider the following inequalities

$$\begin{aligned}&(\tau_{wu}^* - \hat{\tau}_{wu}^*)(\hat{\tau}_{wu}^* - \tau_{wu}^0)\\ \le &-\frac{1}{2}(\hat{\tau}_{wu}^* - \tau_{wu}^*)^2 + \frac{1}{2}(\tau_{wu}^* - \tau_{wu}^0)^2\end{aligned} \tag{56}$$

Similarly,

$$\begin{aligned}&(\tau_{wr}^* - \hat{\tau}_{wr}^*)(\hat{\tau}_{wr}^* - \tau_{wr}^0)\\ \le &-\frac{1}{2}(\hat{\tau}_{wr}^* - \tau_{wr}^*)^2 + \frac{1}{2}(\tau_{wr}^* - \tau_{wr}^0)^2\end{aligned} \tag{57}$$

Applying the lemma of [27], for any $\varepsilon_j > 0$, $\varpi_j \in \mathrm{R}(j = 1, 2)$, there is $0 \le |\varpi_j| - \varpi_j \tan(\varpi_j/\varepsilon_j) \le 0.2785\varepsilon_j$.

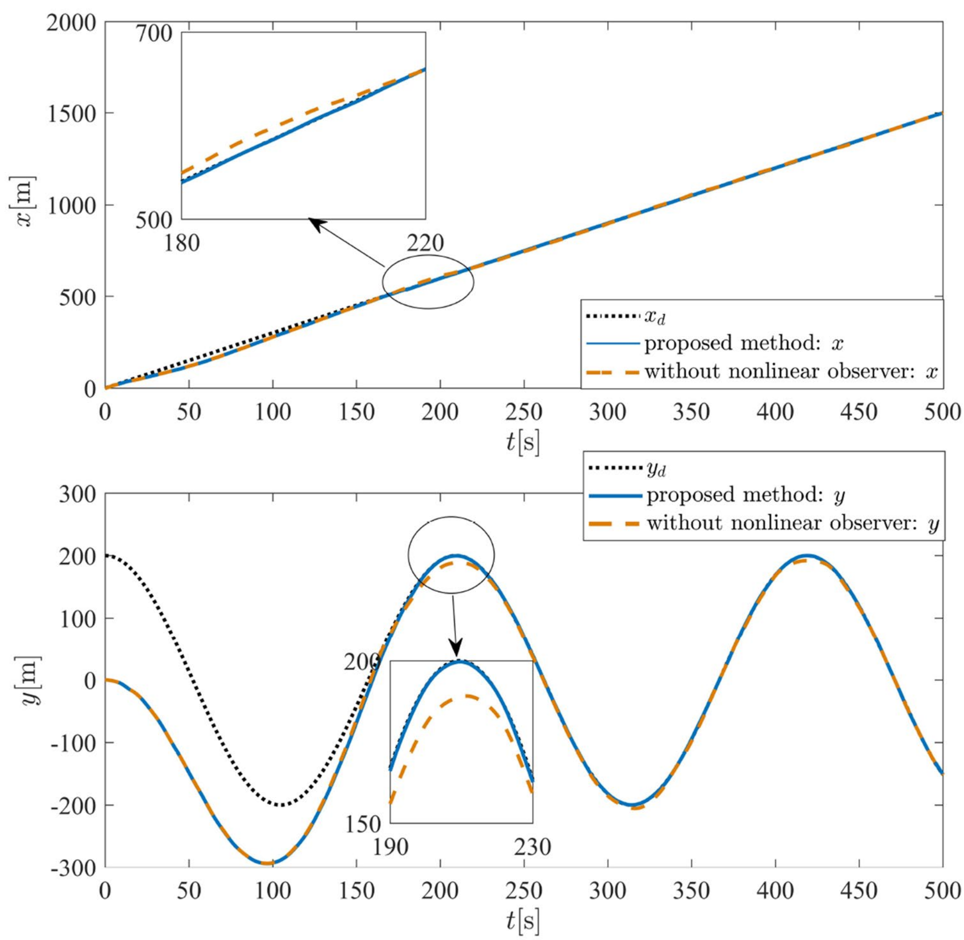

Fig. 8 The curves of ship position

Fig. 9 The surge, sway and yaw velocities of ship

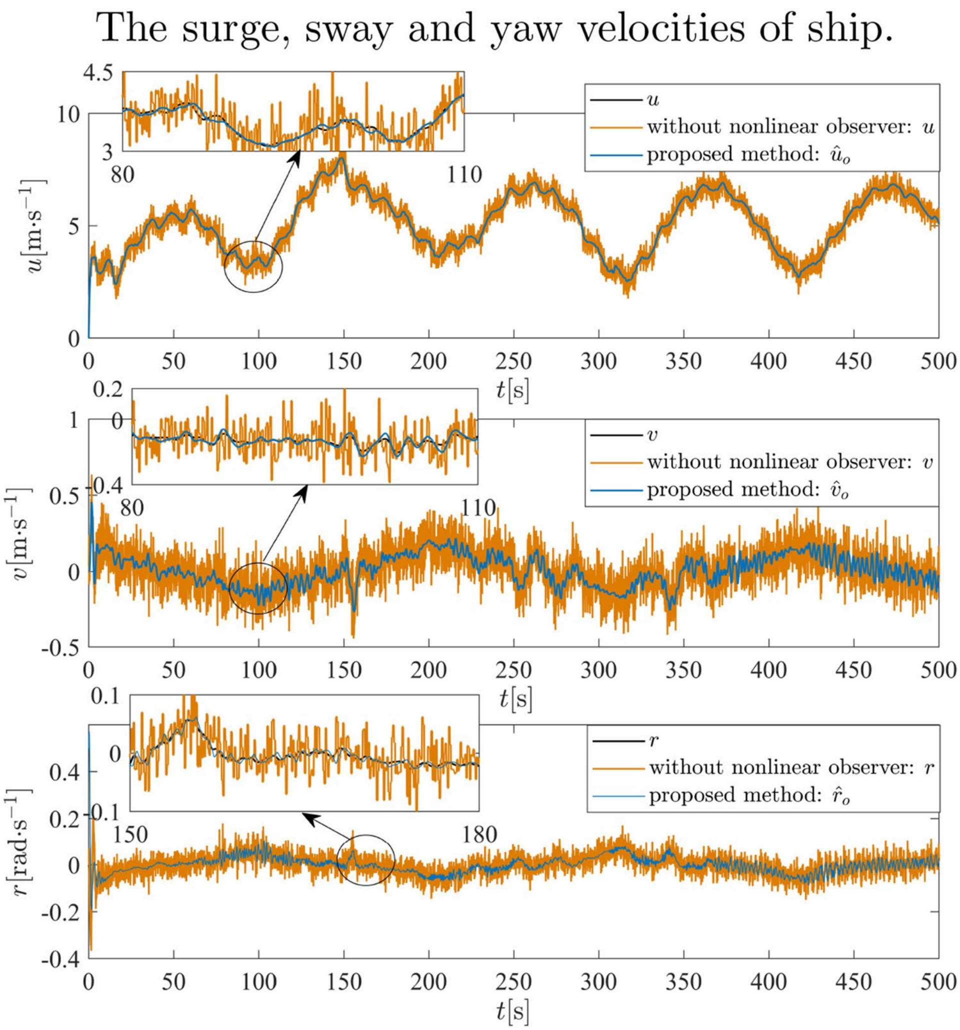

Substitude Eqs. 56, 57 into Eq. 55, we can get

$$
\begin{aligned}
\dot{V} \leq & -k_1 e_x^2 - k_2 e_y^2 - k_3 \bar{u}_e^2 - k_4 \alpha_e^2 - k_5 \bar{r}_e^2 \\
& - \left(\frac{1}{T} - \omega\right) \boldsymbol{Y}^{\mathrm{T}} \boldsymbol{Y} - \frac{\sigma_1}{2}\left(\hat{\tau}_{wu}^* - \tau_{wu}^*\right)^2 \\
& - \frac{\sigma_2}{2}\left(\hat{\tau}_{wr}^* - \tau_{wr}^*\right)^2 + 0.2785\varepsilon_1 \tau_{wu}^* + 0.2785\varepsilon_2 \tau_{wr}^* \\
& + \frac{\sigma_1}{2}\left(\tau_{wu}^* - \tau_{wu}^0\right)^2 + \frac{\sigma_2}{2}\left(\tau_{wr}^* - \tau_{wr}^0\right)^2 \\
& + \frac{N_u^2}{4\omega} + U\alpha_e\delta + \mu_1 + \mu_2 + 1 \\
= & -\mu V + C
\end{aligned}
\tag{58}
$$

where

$$
\mu = \min\left\{2k_1, 2k_2, 2k_3, 2k_4, 2k_5, 2(1/T - \omega), \sigma_1, \sigma_2\right\}
$$

$$
\begin{aligned}
C = & \, 0.2785\varepsilon_1 \tau_{wu}^* + 0.2785\varepsilon_2 \tau_{wr}^* \\
& + \frac{\sigma_1}{2}\left(\tau_{wu}^* - \tau_{wu}^0\right)^2 + \frac{\sigma_2}{2}\left(\tau_{wr}^* - \tau_{wr}^0\right)^2 \\
& + \frac{N_u^2}{4\omega} + U\alpha_e\delta + \mu_1 + \mu_2 + 1 \\
& (1/T - \omega) > 0, 2k_3 - 1 > 0, 2k_5 - 1 > 0
\end{aligned}
$$

So

$$
0 \leq V(t) \leq \frac{C}{\mu} + \left[V(0) - \frac{C}{\mu}\right] e^{-\mu t} \tag{59}
$$

From Eq. 59, it gives

$$
\lim_{t \to \infty} V = \frac{C}{\mu} \tag{60}
$$

Eq. 60 means that the upper bound of $V(t)$ convergence value is C/μ. According to Eq. 55, the ship control system signals $e_x, e_y, \bar{u}_e, \alpha_e, \bar{r}_e, \boldsymbol{Y}, \tilde{\tau}_{wu}^*, \tilde{\tau}_{wr}^*$ are uniformly ultimately bounded

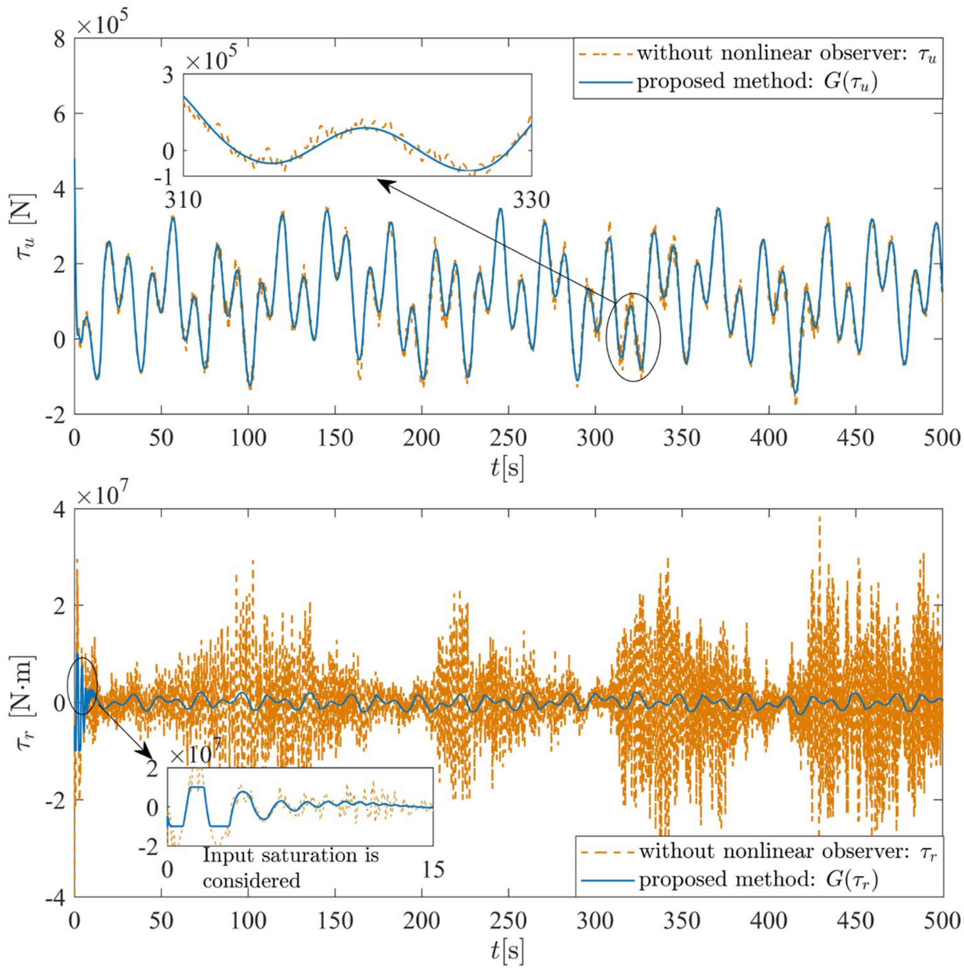

Fig. 10 The comparison curves of control inputs

(UUB). Thus, x_e and y_e are bounded, which can determine all error signals in the closed-loop system are UUB. □

6 Simulation results

In this section, we carry out the simulations of the circular and sine trajectories to demonstrate the effectiveness of the designed controller by a ship named "BAY CLASS" [32]. The ship has a length of 38 m, a mass of $m = 118 \times 10^3$kg ,and other parameters are shown in Table 1. The control parameters are shown in Table 2.

The force and moment of external environmental disturbances are taken as:

$$\begin{bmatrix} \tau_{wu} \\ \tau_{wv} \\ \tau_{wr} \end{bmatrix} = \begin{bmatrix} 1 \times 10^5(\sin(0.2t) + \cos(0.5t)) \\ 1 \times 10^2(\sin(0.1t) + \cos(0.4t)) \\ 1 \times 10^6(\sin(0.5t) + \cos(0.3t)) \end{bmatrix}$$

To further illustrate the superiority of the proposed method, we evaluated the tolerance of the algorithm to noise velocity of measurement, the ship's velocity with measurement noise is $\upsilon = \upsilon + \Xi$, where the power of band-limited white noise Ξ is $[0.01, 0.001, 0.001]^{\mathrm{T}}$ and its sample time is set as $[0.1, 0.1, 0.5]^{\mathrm{T}}$. In this case, we performed simulations with the same control parameters and initial conditions. Furthermore, simulation comparisons are taken with the benchmark method (without nonlinear observer and input saturation).

6.1 Simulation of circular trajectory

Set the desired trajectory: x_d=300$*\sin(0.03t)$, y_d=300 $*\sin(0.03t)$. The initial values of the ship are given to be $x(0)$=0m, $y(0)$=0m, ψ=0.3rad, $u(0)$=0m/s, $v(0)$=0m/s, r(0)=0rad/s.

Fig. 2 shows the simulation diagram of circular trajectory tracking and Fig. 3 shows the position of the ship. We can see from the two figures that the proposed method enables the ship to accurately track the desired trajectory. However, the ship of the comparison method without the nonlinear observer is shifted during tracking due to measurement noise interference. Fig. 4 shows the real values, the actual measurements, and the observer estimation values of ship

Fig. 11 External environmental disturbances and its upper bound

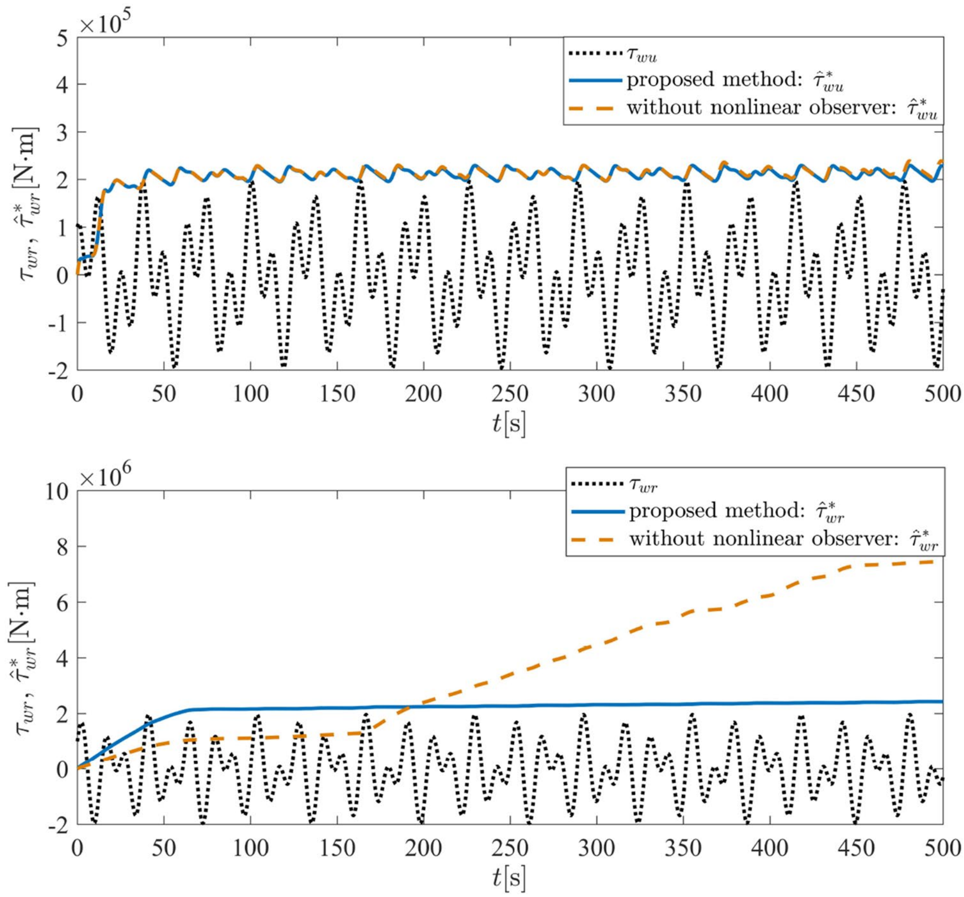

velocities. From the figure, it can be obtained that due to the influence of the measurement noise, the measurements of velocities without the nonlinear observer produces a large error, which affects the tracking accuracy of the ship. However, the proposed method can suppress the noise very well and the velocities estimates are very accurate. From Fig. 5, we can see the comparison curves of control laws. In the early stages of tracking, the control inputs of the proposed method satisfies the input saturation. Therefore, the effectiveness of the designed compensation system can be seen in the fact that the system is still stable in the presence of input saturation. However, the control inputs of the compared methods without the nonlinear observer does not meet the input saturation requirement and the control input varies considerably due to noise, which tends to increase the physical losses of the actuator. Fig. 6 illustrates the upper bound estimation of external disturbances. we can see that the upper bound of the disturbances is well approximated by the proposed method, but the comparison method has a large deviation in the approximation process due to the noise. Thus the designed controller has great robustness against the external disturbances.

6.2 Sine tracking simulation

To further demonstrate the effectiveness of the designed controller in this paper, the circular trajectory is changed to the sine trajectory: $x_d = 3*t$, $y_d = 200*\sin(0.03t)$. The initial values of the ship are given to be $x(0)$=0m, $y(0)$=0m, ψ=0rad, $u(0)$=0m/s, $v(0)$=0m/s, $r(0)$=0rad/s.

In Fig. 7 and Fig. 8, the simulation diagram of sine trajectory tracking and ship positions are shown. We can see from the two figures that the proposed method enables the ship to accurately track the desired trajectory. However, the ship of the comparison method without the nonlinear observer is shifted during tracking due to the measurement noise interference. From Fig. 9, we can see the real values, the actual measurements, and the observer estimation values of ship velocities. It can be obtained that due to the influence of the measurement noise, the measurements of velocities without the nonlinear observer produce a large error, which affects the tracking accuracy of the ship. However, the proposed method can suppress the noise very well and the velocities estimates are very accurate. Fig. 10 shows the comparison curves of control laws. In the early stages of tracking, the control inputs of the proposed method satisfies the input saturation. Therefore, the effectiveness of the designed compensation system can be seen in the fact that the system is still stable in the presence of input saturation. However, the control inputs of the compared methods without the nonlinear observer do not meet the input saturation requirement and the control input varies considerably due to noise, which tends to increase the physical losses of the actuator. In Fig. 11, we can see that the upper bound of the disturbances is well approximated by the proposed method, but the comparison method has a large deviation in the approximation process due to the noise. Thus the designed controller has a great robustness against the external disturbances.

7 Conclusion

Aiming at the trajectory tracking control problem of the underactuated ship with input saturation, an adaptive output feedback DSC trajectory tracking controller is designed in this paper. The control laws are designed by the backstepping technique which stabilizes the position errors and velocity errors in the body-fixed frame. Through the Lyapunov stability theory, all error signals in the control laws are UUB. Using the "BAY CLASS" patrol boat as the controlled object, the trajectory tracking simulations are performed for both circular and sine trajectories. The simulation results show that the designed controller has strong robustness to the external disturbances by introducing the adaptive technique. The observer is designed with a nonlinear gain function to estimate unavailable velocities, which can effectively resolve the contradiction between the dynamic quality and control accuracy of the system. The DSC technique is employed which can reduce the computational complexity of the control algorithm. Furthermore, both hyperbolic tangent function and auxiliary system are used to deal with input saturation, which can provide effective theoretical guidance for engineering practice. In the following study, we will consider the error-constrained problem of the ship and limit the position and velocity errors of the ship to allow for accurate tracking.

Acknowledgements The authors are really grateful to editors and reviewers for their comments, which improve the quality of this study. This work was supported in part by the National Natural Science Foundation of China under Grant 51809028 and Grant 51879027, in part by China Postdoctoral Science Foundation under Grant 2020M670733, in part by the Doctoral Start-up Foundation of Liaoning Province under Grant 2019-BS-022, and in part by the Fundamental Research Funds for the Central Universities under Grant 3132019318.

Author contributions ZS: Conceptualization, Supervision. AL: Writing - original draft, Writing-review & editing. LL: Resources. HY: Funding acquisition, Writing-review & editing.

Declarations

Conflict of interest The authors declare that they have no personal competition or interest relationship that could have influenced the work reported in this paper.

References

1. Zhang G, Liu S, Li J, Zhang X (2021) LVS guidance principle and adaptive neural fault-tolerant formation control for underactuated vehicles with the event-triggered input. Ocean Eng. https://doi.org/10.1016/j.oceaneng.2021.108927
2. Wang Y, Shen Z, Wang Q, Yu H (2021) Predictor-based practical fixed-time adaptive sliding mode formation control of a time-varying delayed uncertain fully-actuated surface vessel using RBFNN. ISA Trans. https://doi.org/10.1016/j.isatra.2021.06.021
3. Chwa D (2021) Adaptive neural output feedback tracking control of underactuated ships against uncertainties in kinematics and system matrices. IEEE J Ocean Eng 46(3):720–735
4. Do KD, Jiang ZP, Pan J (2002) Universal controllers for stabilization and tracking of underactuated ships. Syst Control Lett 47:299–317
5. Yoo SJ, Park JB, Choi YH (2009) Adaptive dynamic surface control for disturbance attenuation of nonlinear systems. Int J Control Autom Syst 7:882–887
6. Zhu G, Du J, Kao Y (2018) Command filtered robust adaptive NN control for a class of uncertain strict-feedback nonlinear systems under input saturation. J Franklin Inst 355:7548–7569
7. Liu YJ, Wang W (2012) Adaptive output feedback control of uncertain nonlinear systems based on dynamic surface control technique. Int J Robust Nonlinear 22(9):945–958
8. Liu Z (2017) Ship adaptive course keeping control with nonlinear disturbance observer. IEEE Access 99(5):17567–17575
9. Sun L, Zheng Z (2015) Nonlinear adaptive trajectory tracking control for a stratospheric airship with parametric uncertainty. Nonlinear Dyn 82(3):1–12
10. Yu C, Xiang X, Lapierre L, Zhang Q (2017) Nonlinear guidance and fuzzy control for three-dimensional path following of an underactuated autonomous underwater vehicle. Ocean Eng 146(1):457–467
11. Zhu G, Ma Y, Li Z, Malekian R, Sotelo M (2021) Adaptive neural output feedback control for MSVs with predefined performance. IEEE Trans Veh Techonl 70(4):2994–3006
12. Liang K, Lin X, Chen Y, Li J, Ding F (2020) Adaptive sliding mode output feedback control for dynamic positioning ships with input saturation. Ocean Eng. https://doi.org/10.1016/j.oceaneng.2020.107245
13. Peng Z, Wang J (2018) Output-feedback path-following control of autonomous underwater vehicles based on an extended state observer and projection neural networks. IEEE Trans Syst Man Cybern-Syst 48(4):535–544
14. Deng Y, Zhang X (2021) Event-triggered composite adaptive fuzzy output-feedback control for path following of autonomous surface vessels. IEEE Trans Fuzzy Syst 29(9):2701–2713
15. Doyle JC, Stein G (2007) Robustness with observers. IEEE Trans Autom Control 24(4):607–611
16. Ngongi WE, Du JL (2014) A high-gain observer-based pd controller design for dynamic positioning of ships. Appl Mech Mater 490:803–808
17. Du J, Yang Y, Wang D, Guo C (2013) A robust adaptive neural networks controller for maritime dynamic positioning system. Neurocomputing 110:128–136

18. Du J, Hu X, Liu H, Chen CLP (2015) Adaptive Robust Output Feedback Control for a Marine Dynamic Positioning System Based on a High-Gain Observer. IEEE Trans Neural Netw Learn Syst 26:1–12
19. Tee KP, Ge SS (2006) Control of fully actuated ocean surface vessels using a class of feedforward approximators. IEEE Trans Control Syst Technol 14(4):5640–5647
20. Do KD, Jiang ZP, Pan J (2005) Global partial-state feedback and output-feedback tracking controllers for underactuated ships. Syst Control Lett 54:1015–1036
21. Do KD, Pan J (2004) State- and output-feedback robust path-following controllers for underactuated ships using Serret-Frenet frame. Ocean Eng 31:587–613
22. Liu L, Wang D, Peng Z (2019) State recovery and disturbance estimation of unmanned surface vehicles based on nonlinear extended state observers. Ocean Eng 171:625–632
23. Chwa D (2011) Global tracking control of underactuated ships with input and velocity constraints using dynamic surface control method. IEEE Trans Control Syst Technol 19(6):1357–1370
24. Du J, Hu X, Krstić M, Sun Y (2016) Robust dynamic positioning of ships with disturbances under input saturation. Automatica 73(7):207–214
25. Hu Q, Shao X, Zhang Y, Guo L (2018) Nussbaum-type function-based attitude control of spacecraft with actuator saturation. Int J Robust Nonlinear Control 28(1):2927–2949
26. Zhu G, Du J (2020) Global robust adaptive trajectory tracking control for surface ships under input saturation. IEEE J Ocean Eng 45(2):442–450
27. Huang J, Wen C, Wang W, Song YD (2015) Global stable tracking control of underactuated ships with input saturation. Syst Control Lett 85:1–7
28. Liu C, Chen CLP, Zou Z, Li T (2017) Adaptive NN-DSC control design for path following of underactuated surface vessels with input saturation. Neurocomputing 267:466–474
29. Zheng Z, Sun L (2016) Path following control for marine surface vessel with uncertainties and input saturation. Neurocomputing 177:158–167
30. Fossen TI (2002) Marine Control Systems: Guidance, Navigation, and Control of Ships, Rigs and Underwater vehicles. In: Marine Cybernetics, Trondheim, Norway Number NO985 195 005 MVA, ISBN: 82 92356 00 2. https://www.marinecybernetics.com
31. Swaroop D, Hedrick JK, Yip PP, Gerdes JC (2000) Dynamic surface control design for a class of nonlinear systems. IEEE Trans Automat Contr 45(10):1893–1899
32. Do KD, Jiang ZP, Pan J (2004) Robust adaptive path following of underactuated ships. Automatica 40(6):929–944